Progress In Electromagnetics Research Letters, Vol. 109, 93–101, 2023

Design of a W-Band Dual-Circular-Polarization Monopulse Cassegrain Antenna for Polarization Detection of Radar Target

Xin Li*, Kun Gao, Ying-Chao Zhao, Jian Yuan, Jie Cheng, and Yuan-Yuan Wang

Abstract—A W-band dual-circular-polarization (dual-CP) monopulse Cassegrain antenna for polarization detection of radar target is presented in this letter. The proposed antenna consists of a main reflector, a sub-reflector, a dual-CP feed source based on the septum polarizer, and a comparator. Two orthogonal circular-polarized signals [left-hand circular polarization (LHCP) and right-hand circular polarization (RHCP)] electromagnetic wave can be transmitted and received simultaneously by this antenna. The principle of the antenna is introduced and analyzed, and then a prototype of the antenna is simulated, fabricated, and measured. Measured results are in good agreement with the simulated ones. At 94 GHz, the gains of the LHCP and RHCP sum beam (SUM beam) are 38.6 dBi and 38.8 dBi counting the insertion loss of the comparator, which indicates that the radiation efficiency is better than 44.2%. The 3-dB beamwidth is about 1.5° with a sidelobe level (SLL) of −16.6 dB, and the axial ratio is lower than 1.43. A null depth of −26 dB for the difference beam (DIFF beam) is observed, and the gain ratio between the LHCP monopulse beams is 5.9 dB. Measured results demonstrate that the proposed antenna is very applicable in the polarization detection of radar target at W-band.

1. INTRODUCTION

Recently, due to the development of millimeter-wave components, radar working at W-band with narrow beam, compact size, and high accuracy in angle measurement is widely employed in many areas, such as target detection systems, meteorological radar, and security inspection system. Compared to the single polarization antenna, the dual-polarization antenna is preferred [1–3] due to its ability to suppress polarization mismatch and multipath interference. Dual-polarization radar systems can get extra information like polarization scattering matrix from the echo in polarization domain besides conventional time domain and frequency domain, which is very helpful in target classification and identification, and greatly enhances the capability of radar target detection [4–6]. Therefore, a dual-polarization sensor working at W-band is of great significance.

Compared to a linear polarization antenna, a circular polarization antenna has better performance in transmission through the rain and frog. Meanwhile, circular polarization (CP) antenna can receive the echo with any polarization angle. Therefore, dual-CP monopulse antenna is more critical in a W-band dual-polarization detection system. Several dual-CP antennas have been proposed in the literature [7–10], including microstrip array [7], substrate integrated waveguide (SIW) antenna [8], and horn antenna [9, 10]. However, SUM and DIFF patterns cannot be generated simultaneously by these dual-CP antennas, because the monopulse comparator is difficult to design in the restricted space, where the distance between array elements should be less than λ (wavelength), especially at W-band. Antennas based on the quasi-optic theory such as lens [11], reflectarrays [12, 13], and reflectors [14–16] are potentially to be applied in the dual-CP monopulse antenna application at W band. Replacing the

Received 12 January 2023, Accepted 28 February 2023, Scheduled 8 March 2023

* Corresponding author: Xin Li (xdlixin@foxmail.com).

The authors are with the Department of Microwave Engineering, Xi'an Electronic Engineering Research Institute, Xi'an, Shaanxi 710100, China.

feeding horn of the dielectric lens with the dual-CP monopulse feed source [11] can easily make the antenna satisfy the demands, but the dielectric lens antenna suffers great weight and long longitudinal dimension. Reflectarray can generate dual-CP with the advantages of low cost and low weight, which can be easily designed at W-band by minifying the dimensions proportionally. However, the transmission loss is introduced by the longer feed waveguide because the T/R modulates are generally placed behind the array [12, 13]. A W band parabolic antenna with a dual-CP monopulse feeder is researched [14]. However, it is not high in radiation efficiency due to the blockage introduced by the extra space of the comparator. To decrease the blockage loss and longitudinal dimension, a Cassegrain antenna with a sequential rotate polarization feed is developed [15, 16]. By using specific settings of the amplitude and phase, linear (Horizontal and Vertical) or circular (Left and Right) monopulse patterns are produced. However, four additional phase shifters are needed to adjust the phase of the polarization feed ports, which introduces considerable insertion loss and makes the system more complex, less efficient, and the LHCP and RHCP patterns cannot be radiated simultaneously.

To overcome these disadvantages of antennas in the works [7–16] in dual-CP monopulse applications, a dual-CP monopulse Cassegrain antenna is presented in this letter. By employing the septum polarizer-based feed source and the comparator for dual-CP, the antenna can radiate the monopulse patterns with LHCP and the sum patterns with RHCP simultaneously, which has the advantages of low weight and profile, and high radiation efficiency. In Section 2, the configurations and detailed design theory are introduced. Measured and simulated results are compared and discussed in Section 3, and the conclusion is given in Section 4.

2. ANTENNA DESIGN

The proposed Cassegrain antenna is demonstrated in Fig. 1, which consists of a parabolic main reflector, a hyperbolic sub-reflector, the comparator, and a feed source. As shown in this figure, the main reflector and sub reflector share a common focal point O', and another focal point of the sub reflector is the phase center of the feed source. The main reflector has a projected aperture in the *xoy* plane with a diameter of D_m, and its focal length is F_m. The projected aperture of the hyperbolic sub reflector in *xoy* plane is described as D_s, and the sub reflector edge angle is 2φ. The dimension parameters of the reflector are optimized and obtained by a commercial simulation software HFSSv15 at 94 GHz.

In our application, D_m is limited to 130 mm, and for the realization of high radiation efficiency, F_m/D_m is set as 0.46 ($F_m = 60$ mm), which usually ranges $0.3 \sim 0.5$. Empirical formula $D_s = \sqrt{2F_m\lambda/k}$ given in [17] is employed to obtain the diameter of the sub reflector D_s, where λ and k are the wavelength and blockage coefficient, respectively. To reduce the blockage and diffraction introduced by the sub

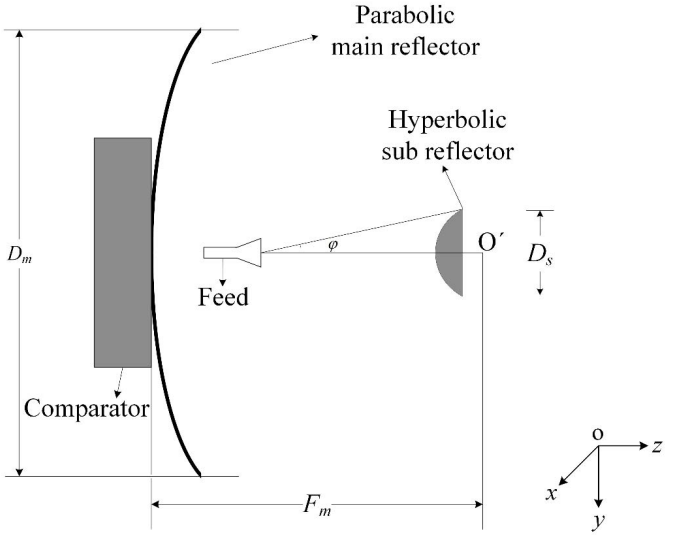

Figure 1. Geometry of the Cassegrain antenna system.

reflector, we set D_s as 23 mm and φ as 20°. Thus, the contours of the main and sub reflectors in the yoz plane satisfy $z = 240y^2$ and $z^2/9.9472 - y^2/16.8292 = 1$, respectively.

2.1. Design of the Septum Polarizer-Based Feed Source

The proposed feed source consists of four septum polarizers, which are arrayed as shown in Fig. 2. The septum polarizer is a good candidate for dual-CP applications due to its advantages of wideband, low axial ratio, and simple structure. A thin wall is placed in the middle of the square waveguide, and the excitation port is divided in two. Two orthogonal circular polarization signals can be excited by the two ports of the septum polarizer. As can be seen in this figure, the septum polarizer is composed of a rectangular waveguide section, a septum section, and a square waveguide section.

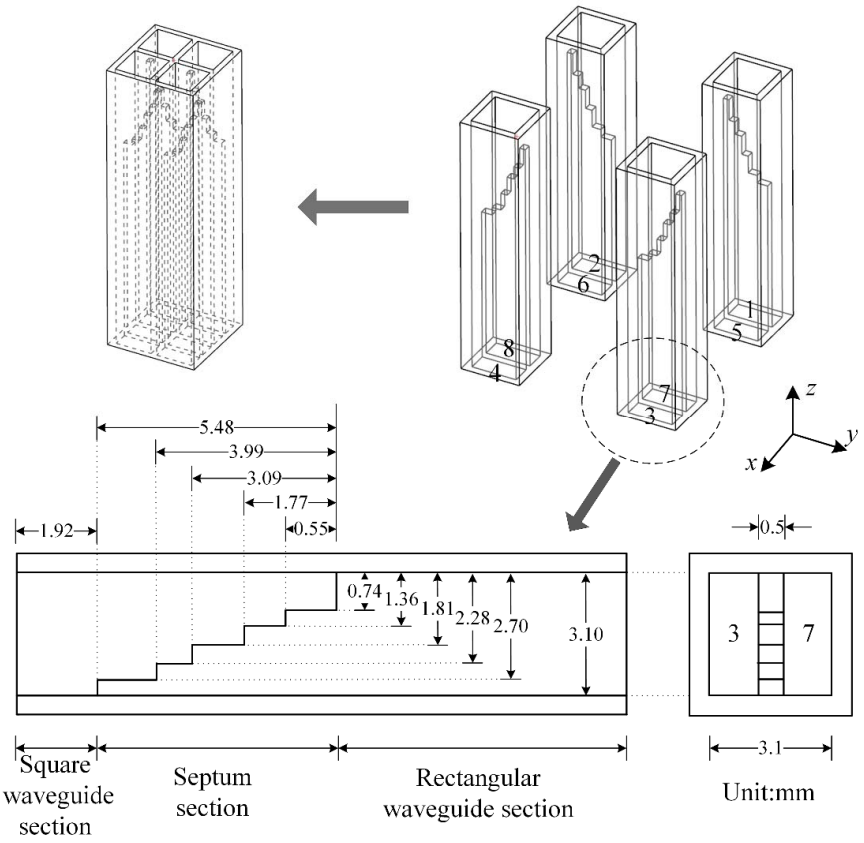

Figure 2. The structure of the feed based on the septum polarizer.

Figure 3 is the schematic diagram of working principle of the septum polarizer. According to the waveguide transmission theory, TE10 mode is the fundamental mode in the rectangular waveguide section when port 1 or port 2 is excited, and the corresponding electric field is annotated as E. The excited TE10 mode will be converted to TE10 and TE01 modes (annotated as E1 and E2) by the septum section. The TE10 and TE01 modes are orthogonal, and they can propagate in the square waveguide section. It is well known that the circular polarization can be generated when the horizontal and vertical components of the electromagnetic wave are with the same amplitude and ±90° phase shift. A five step spectrum wall is employed to finish the mode transformation. By adjusting the dimensions of the step spectrum properly, the propagated TE10 (E1) and TE01 (E2) modes are tuned to satisfy the condition of CP within the desired frequency band. A phase difference of 90° and equal amplitude between E2 and E1 can be achieved. Thereby, port 1 can generate LHCP, and port 2 can generate RHCP. The LHCP and RHCP electromagnetic waves can be radiated by the stepped septum polarizer simultaneously.

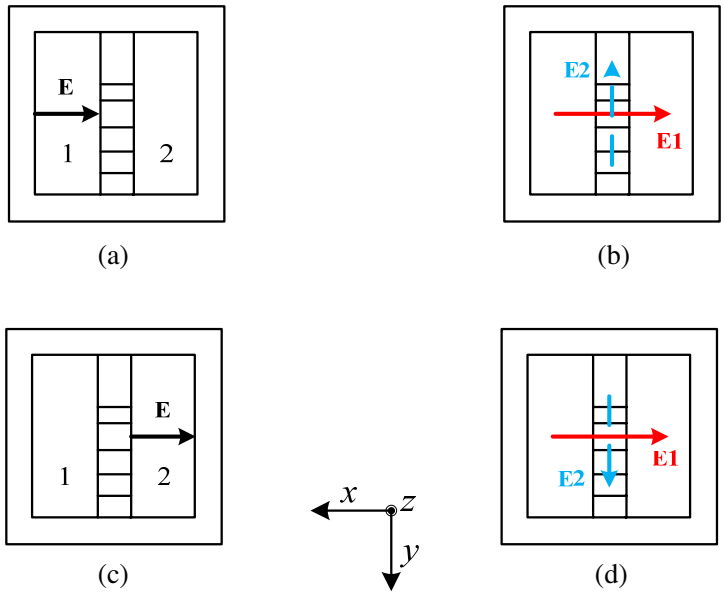

Figure 3. Schematic diagram of working principle of the septum polarizer: (a) TE10 mode at port 1; (b) TE10 and TE01 mode excited by port 1; (c) TE10 mode at port 2; (d) TE10 and TE01 mode excited by port 2.

As illustrated in Fig. 2, there are eight excitation ports represented as 1–8 for the proposed feed source. The LHCP is generated when ports 1–4 are excited, and the RHCP can be generated by the excitation of ports 5–8. The aperture size of the square waveguide is adjusted to make the 10-dB beamwidth of the feed source match the sub reflector edge angle 2φ, which is closely correlated to the size of the feed source aperture. The optimized dimensions of the septum polarizers are also listed in Fig. 2.

2.2. Design of the Dual-CP Monopulse Comparator

The dual-CP monopulse comparator is achieved by the waveguide form due to its low transmission lost at W band. The diagram of the comparator is shown in Fig. 4, where the LHCP comparator is in Fig. 4(a) and RHCP feed network in Fig. 4(b), respectively. Due to the advantages of high isolation and broad band between the two output ports, a planar magic-T is employed to achieve the sum and difference functions simultaneously, which is expressed as $\sum$ and Δ in this figure. A T-junction power divider is also used as the sum unit due to its easy fabrication. As shown in Fig. 4(a), by applying three planar magic-Ts and one T-junction power divider, the monopulse comparator for LHCP is achieved. When ports P1–P3 are excited, monopulse patterns can be radiated with LHCP. The difference between the received amplitudes and phase by the monopulse beam of LHCP can be used to measure the direction of the target. The SUM beam of LHCP can be applied to measure the range of the target. Therefore, the measurement of direction and range of radar target can be achieved by the comparator of LHCP independently. It can satisfy the main demand of the traditional radar. Three T-junctions are applied to produce the SUM pattern for RHCP as shown in Fig. 3(b). It should be noticed that only the SUM pattern is radiated for the RHCP. The monopulse comparator for RHCP can also be designed by adding several planar magic-Ts and T-junction power dividers if necessary. The antenna proposed in this paper is designed to work in two orthogonal polarizations, LHCP and RHCP. By receiving the echo of target by the LHCP and RHCP SUM beams, information like the polarization scattering matrix of target in polarization domains can be obtained, which is beneficial for target classification and identification [4]. By the application of the proposed dual-CP monopulse comparator, the capability of the radar in target detection has been greatly enhanced. The simulation model of the proposed comparator is shown in Fig. 5, and the key components like planar magic-T and T-junction power divider are marked in this

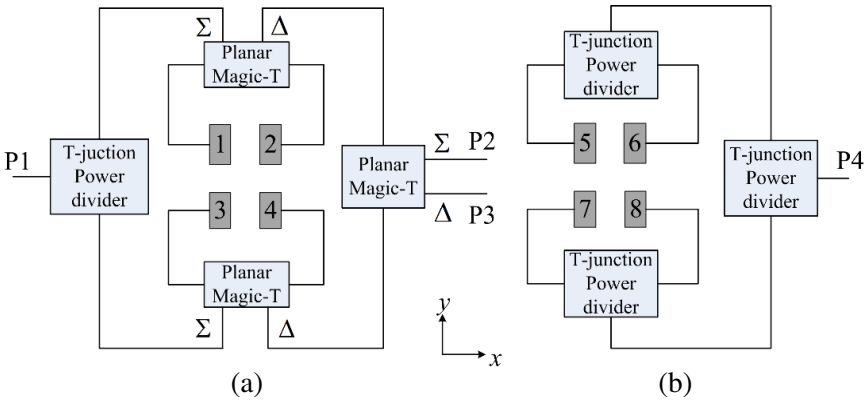

Figure 4. Diagram of the proposed comparator: (a) The LHCP monopulse comparator; (b) The RHCP comparator.

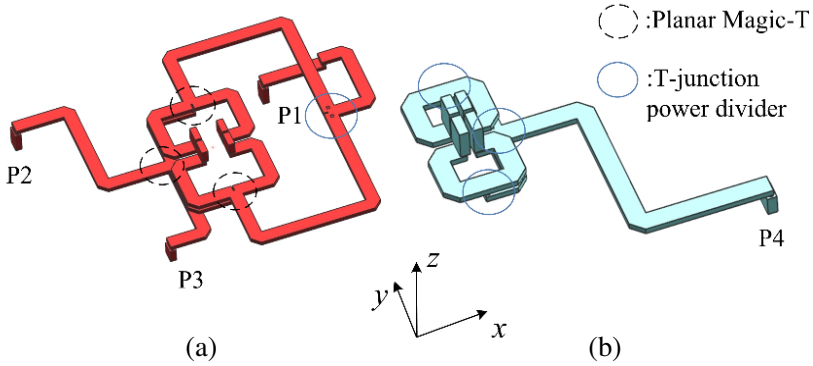

Figure 5. Simulation model of the proposed comparator: (a) The LHCP monopulse comparator; (b) The RHCP comparator.

Table 1. Phase values and radiation patterns for each port of the proposed comparator (unit: °).

Port	1	2	3	4	Patterns
P1	0	180	0	180	DIFF-pattern: LHCP-*xoz* plane
P2	0	0	0	0	SUM-pattern: LHCP
P3	0	0	180	180	DIFF-pattern: LHCP-*yoz* plane
Port	5	6	7	8	Patterns
P4	0	0	0	0	SUM-pattern: RHCP

figure to understand the design principle better. The relationship between the excitations of comparator ports P1–P4 and the phase values of polarizer ports 1–8 is given in Table 1. Based on this conclusion, the corresponding radiation patterns of the excitations for ports P1–P4 are determined, which are also listed in this table. As listed in this table, the comparator can produce monopulse patterns in the *xoz* plane and *yoz* plane for LHCP and the SUM pattern for RHCP simultaneously.

As shown in Fig. 6(a), the LHCP and RHCP monopulse comparators are designed together to save space. The wide wall of the rectangular waveguide is 3.1 mm to match the dimension of the feed source, and the narrow wall of the waveguide is compressed to 0.8 mm for low profile and easy matching. The four output ports P1–P4 are standard WR-10 waveguide, whose aperture size is 2.54 mm × 1.27 mm. The simulation result indicates that the insertion loss of the proposed comparator is about 0.49 dB for LHCP and 0.41 dB for RHCP. The lower insertion loss of the comparator is attribute to the application

of waveguide. Simulation result demonstrates that the amplitude and phase unbalance are within 0.22 dB and 2 deg, respectively. Within the frequency band from 92 to 96 GHz, the S_{11} of ports P1–P4 are less than −15 dB, and port isolations are better than 32 dB. The rectangular waveguide cavity and the slot are milled from the machined aluminum slices structure by a numerical control machine tool. As shown in Fig. 6(b), the whole comparator structure is divided into four layers in order to facilitate the manufacture. These four layers of machined aluminum structure are soldered to form the whole proposed dual-CP comparator, and its thickness is only 10 mm. A photograph of the prototype of the comparator in shown in Fig. 6(c).

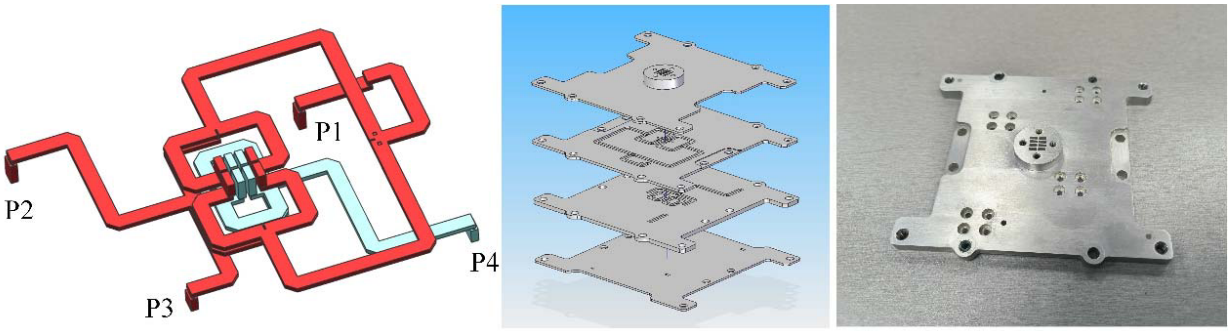

Figure 6. Models of the proposed comparator: (a) The simulation model; (b) The exploded views of the machining model; (c) The prototype of the proposed comparator.

3. MEASUREMENT RESULTS AND DISCUSSION

A prototype of the proposed antenna is fabricated and measured as shown in Fig. 7. The measurement is based on the entire antenna system including the sub-reflector, feed source, main reflector, and comparator. As illustrated in Fig. 8, the measured S_{11} of ports P1–P4 are all below −12.8 dB within the frequency range from 92 to 96 GHz.

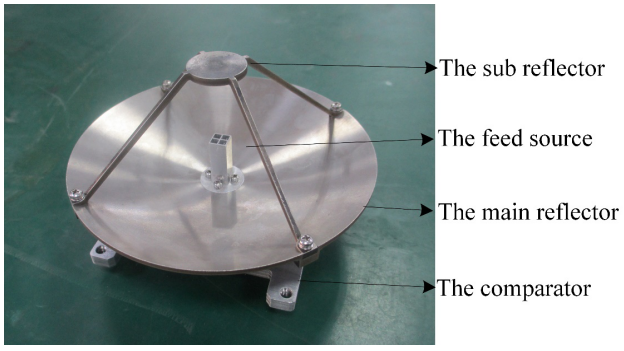

Figure 7. The photograph of the fabricated prototype.

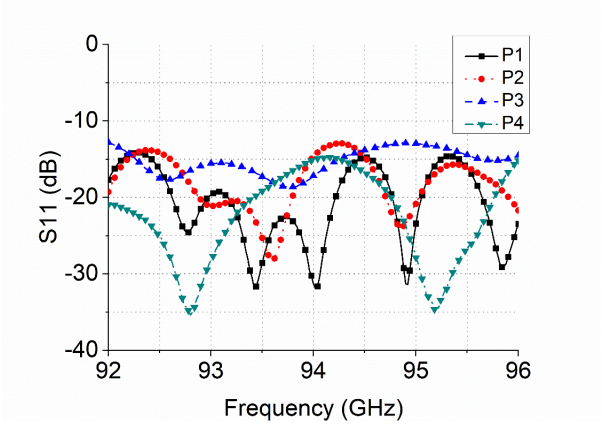

Figure 8. Measured S_{11} of the proposed antenna.

The simulated and measured normalized monopulse patterns with LHCP at 94 GHz are compared and shown in Fig. 9, and they are in a good agreement. For the SUM pattern in both the *xoz* and *yoz* planes, the gain is 38.6 dBi; the beamwidth with 3-dB is about 1.5°; and the SLL is less than −16.6 dB. For the DIFF pattern, it is observed that the null depth is −40 dB in the *xoz* plane and −26 dB in the

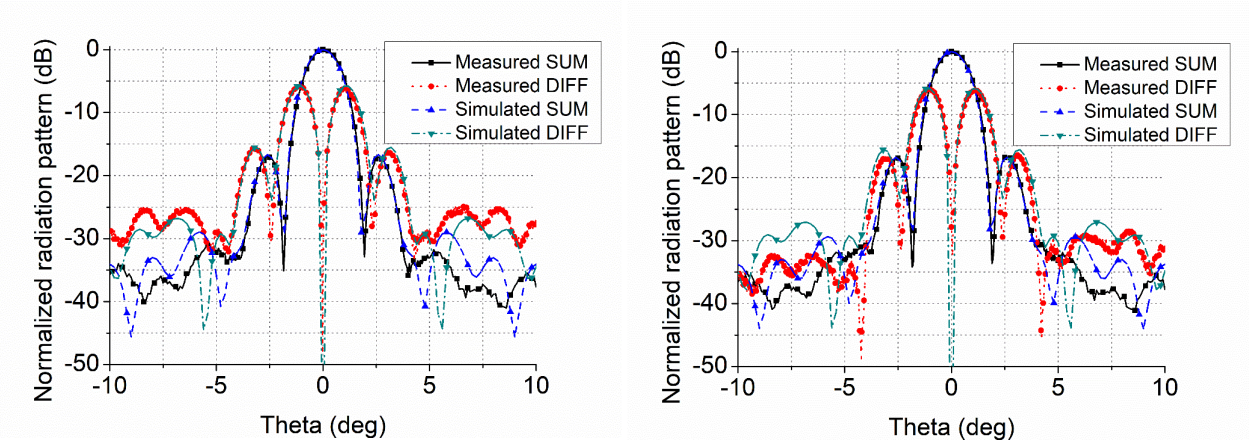

Figure 9. Normalized measured and simulated monopulse patterns with LHCP of the proposed antenna: (a) in the *xoz* plane; (b) in the *yoz* plane.

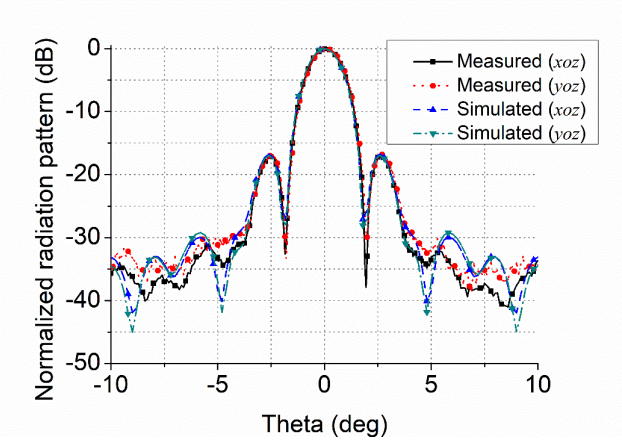

Figure 10. Normalized measured and simulated patterns with RHCP of the proposed antenna.

yoz plane. The unbalance of two peaks for the DIFF pattern is less than 0.4 dB and 0.3 dB in the *xoz* plane and *yoz* plane, respectively. Furthermore, the gain ratios of the monopulse patterns are lower than 5.9 dB. A good performance of the antenna excited by port P4 with RHCP can also be observed as shown in Fig. 10. The gain is 38.8 dBi; the beamwidth with 3-dB is about 1.5°; and the SLL is below −16.8 dB, whose performance is mainly similar to the LHCP SUM beam. The measured axial ratio and gain of the proposed antenna system for LHCP and RHCP within the frequency range from 92 to 96 GHz are shown in Fig. 11. It is observable from this figure that the gain of the antenna for LHCP is better than 38.0 dBi, and that for RHCP is better than 38.1 dBi within the frequency range. The axial ratio of the LHCP and RHCP patterns is below 1.56 dB, which demonstrates that the proposed antenna has a good performance in circular polarization.

The performances of different W-band monopulse antennas are compared and listed in Table 2. The aperture sizes of the antennas are different. To be fair, the total radiation efficiencies of the entire antenna systems are compared. It is worth to notice that the insertion loss of W-band comparator is taken into account for fair comparison of antenna gains in this table, which are eliminated in [15, 16]. As shown in this table, the same waveguide comparators are applied in [15] and [16]. It is worth noting that four additional phase shifters are needed for this comparator to adjust the phase of the polarization feed ports, which introduce the insertion loss about 1 dB. A SIW monopulse feeder, which consists of a SIW slot antenna array and a SIW comparator, is employed as the feed source of the parabolic reflector in [14]. The size ratio between the blockage and the reflector is about 0.29, and the simulated blockage

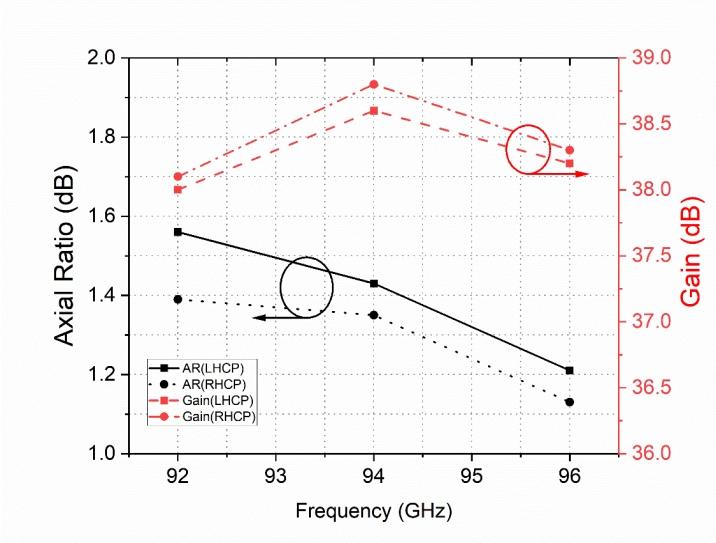

Figure 11. Measured axial ratio and gain of the proposed antenna.

Table 2. Comparison of different dual-CP monopulse antennas working at W band.

Num	Ref. [15]	Ref. [16]	Ref. [14]	This work
Type	Waveguide comparator +horns	Waveguide comparator +patches	SIW comparator +SIW slots	Waveguide comparator +horns
Aperture size (mm)	135	135	140	130
Gain (dBi)	35.1	38.6	35.6	38.6
Total EFF. (%)	18.2	41.2	19.1	44.2

loss is about 1.52 dB, which is one of the main reasons that the radiation efficiency is not very high. Furthermore, the SIW monopulse feeder is excited by the waveguide, and the insertion loss introduced by this transform structure is not to be neglected. For the proposed antenna in our paper, the phase shifters are not needed in the comparator, and the feed source (septum polarizer) is excited by the waveguide comparator directly. Therefore, the insertion loss introduced by the comparator and feed source in our proposed antenna is much lower than those of the antennas in [14–16]. The total radiation efficiency of our antenna for LHCP and RHCP at 94 GHz is 44.2%, which indicates that the proposed antenna can radiate with better aperture efficiency than the antennas in the listed references.

4. CONCLUSION

A W-band dual-CP Cassegrain antenna with monopulse patterns is designed, fabricated, and measured in this letter. By applying a septum polarizer based-feed source and dual-CP monopulse comparator, the proposed antenna can transmit and receive two orthogonal circularly-polarized signals LHCP and RHCP simultaneously. The measured results show a good agreement with the simulated ones. For the LHCP and RHCP at 94 GHz, the 3-dB beamwidths are both about 1.5°, and the SLLs are under −16.6 dB. The gain is better than 38.6 dB with an axial ratio of 1.43 dB, which indicates that the radiation efficiency of the radiated LHCP and RHCP is better than 44.2%. The results demonstrate that the proposed antenna is a good candidate for dual-CP monopulse detector systems at W-band.

REFERENCES

1. Aboserwal, N., J. L. Salazar-Cerreno, and Z. Qamar, "An ultra-compact X-band dual-polarized slotted waveguide array unit cell for large E-scanning radar systems," *IEEE Access*, Vol. 8, 210651–210662, 2020.
2. Wang, Y. and V. Chandrasekar, "Polarization isolation requirements for linear dual-polarization weather radar in simultaneous transmission mode of operation," *IEEE Trans. Geoscience and Remote Sensing*, Vol. 44, 2019–2028, 2006.
3. Lv, J., M. Su, and Y. Liu, "Broadband dual-polarized mm-Wave antenna array with grating structure for mobile devices," *IEEE Trans. Antennas Propagat.*, Vol. 22, 273–277, 2023.
4. Giuli, D., "Polarization diversity in radars," *Proceedings of the IEEE*, Vol. 74, 245–269, 1986.
5. Cloude, S. R. and E. Pottier, "A review of target decomposition theorems in radar polarimetry," *IEEE Trans. Geoscience and Remote Sensing*, Vol. 34, 498–518, 1996.
6. Yin, J., H. Chen, Y. Li, and X. Wang, "Clutter mitigation based on spectral depolarization ratio for dual-polarization weather radars," *IEEE Journal of Selected Topics in Applied Earth Observations and Remote Sensing*, Vol. 14, 6131–6145, 2021.
7. Shen, Y., S. G. Zhou, G. L. Huang, and T. H. Chio, "A compact dual circularly polarized microstrip patch array with interlaced sequentially rotated feed," *IEEE Trans. Antennas Propagat.*, Vol. 64, 4933–4936, 2016.
8. Cheng, Y. J., J. Wang, and X. L. Liu, "94 GHz substrate integrated waveguide dual-CP shared-aperture parallel-plate long-slot array antenna with low sidelobe level," *IEEE Trans. Antennas Propagat.*, Vol. 65, 5855–5861, 2017.
9. Shu, C., J. B. Wang, S. Q. Hu, Y. Yao, J. S. Yu, Y. Alfadhl, and X. D. Chen, "Wideband dual-CP horn antenna for mmWave wireless communications," *IEEE Antennas Wireless Propag. Lett.*, Vol. 18, 1726–1730, 2019.
10. Dong, Y., R. Xu, Y. H. Yang, and S. G. Zhou, "Compact shared-aperture dual-band dual-circularly-polarized waveguide antenna array operating at K/Ka-band," *IEEE Trans. Antennas Propagat.*, Vol. 71, 443–449, 2023.
11. Mahmoud, A. E., W. Hong, Y. Zhang, and A. Kishk, "W-band multilayer perforated dielectric substrate lens," *IEEE Antennas Wireless Propag. Lett.*, Vol. 13, 734–737, 2014.
12. Lorencio, R., J. A. Encinar, R. R. Boix, M. Barba, and G. Toso, "Flat reflectarray that generates adjacent beams by discriminating in dual circular polarization," *IEEE Trans. Antennas Propagat.*, Vol. 67, 3733–3742, 2019.
13. Xu, P., L. Li, R. Li, and H. Liu, "Dual-circularly polarized spin-decoupled reflectarray with FSS-back for independent operating at Ku-/Ka-bands," *IEEE Trans. Antennas Propagat.*, Vol. 69, 7041–7046, 2021.
14. Kou, P. F. and Y. J. Cheng, "A dual circular-polarized extremely thin monopulse feeder at W-band for prime focus reflector antenna," *IEEE Antennas Wireless Propag. Lett.*, Vol. 18, 231–235, 2019.
15. Zheng, P., G. Q. Zhao, S. H. Xu, F. Yang, and H. J. Sun, "Design of a W-band full-polarization monopulse Cassegrain antenna," *IEEE Antennas Wireless Propag. Lett.*, Vol. 16, 99–103, 2017.
16. Zheng, P., B. Hu, S. Xu, and H. Sun, "A W-band high-aperture-efficiency multipolarized monopulse Cassegrain antenna fed by phased microstrip patch quad," *IEEE Antennas Wireless Propag. Lett.*, Vol. 16, 1609–1613, 2017.
17. Volakis, J., *Antenna Engineering Handbook*, 4th Edition, McGraw-Hill, New York, NY, USA, 2007.